

Smolyak algorithm assisted robust control of quantum systems

Zigui Zhang¹, Zibo Miao^{1*}, Yu Chen², Xiu-Hao Deng^{3,4}

^{1*}Mechanical Engineering and Automation, Harbin Institute of Technology, Shenzhen, 518055, China.

²LIGHTSPEED STUDIOS, Tencent, Shenzhen, 518057, China.

³Shenzhen Institute of Quantum Science and Engineering, Southern University of Science and Technology, Shenzhen, 518055, China.

⁴International Quantum Academy, Shenzhen, 518000, China.

*Corresponding author(s). E-mail(s): miaozibo@hit.edu.cn;

Abstract

Efficient and systematic numerical methods for robust control design are crucial in quantum systems due to inevitable uncertainties or disturbances. We propose a novel approach that models uncertainties as random variables and quantifies robustness using the expectation of infidelity. By reformulating the robustness measure as a weighted tensor product quadrature, we employ the Smolyak sparse grid algorithm to develop a parametric robust quantum control scheme. This scheme significantly reduces computational cost while improving accuracy. We demonstrate the effectiveness of our Smolyak algorithm assisted gradient-based methods including **smGOAT** and **smGRAPE** in robust control problems regarding state transfer and quantum gate realization, with ultrahigh fidelity and strong robustness achieved. Our results contribute to improving the reliability and security of quantum computing and communication systems in the presence of real-world imperfections.

Keywords: quantum systems with uncertainties, robust control, Smolyak algorithm

1 Introduction

In the past few decades, theoretical and experimental studies have witnessed rapid development in quantum technologies, including quantum information and computation. Quantum control is crucial to the successful realization of these frontier technologies, which is usually implemented by manipulating the Hamiltonians of quantum systems. In particular, developing a systematic control framework that can robustly drive the dynamics of the quantum system towards the target in the presence of modeled noise or unknown uncertainty remains a challenge [1, 2]. Many efforts have been made to improve the robustness of quantum control in various ways. For example, the geometric correspondence of the evolving manifold, such as curvature, can be exploited to improve the robustness [3–8]. Similarly, noise terms in the expansion of the control objective can be eliminated to a great extent by elaborately constructing the dynamical trajectory of the system [9–11], or by numerical optimization [12–14]. In addition, methods from other perspectives have been proposed, such as dynamical decoupling [15, 16], composite pulses [17, 18] and shortcuts to adiabaticity [19].

In the vast majority of scenarios, the analytic form of control is rather complicated or even does not exist. Even if control signals can be obtained numerically using expansion-based methods, we have to calculate the troublesome high-order expansion to achieve high-level robustness. In this regard, an effective numerical approach without complex calculations to achieve high-level robustness may be a better solution. A promising candidate is the sampling-based (ensemble-based) method [20]. By modeling the uncertainty that inevitably exists in quantum systems as random variables following prescribed distributions, we can evaluate the robustness via expectation of the control objective as a performance index. To this end, the performance index can be approximated by averaging or weighting the samples from the sampling space with different strategies such as equidistant grids [20–22], Monte Carlo [23], or learning-based algorithms [24, 25].

However, the number of samples typically grows exponentially due to the curse of dimensionality, which leads to extreme cost in computation and sentences the method of equidistant sampling to death. Monte Carlo analysis tends to require extensive sampling, which gives rise to significant processing power and time, and the results of Monte Carlo analysis are not easy to interpret. Although the sampling cost can be reduced and an efficient strategy can be appropriately designed by learning-based algorithms, the corresponding sensitivities to configuration, such as modifying and retraining the learning model when dynamics change caused by the time horizon or newly added uncertainty, prevent further generalization. Therefore, a reliable and universal sampling strategy is still in need.

Inspired by sampling-based algorithms, in this paper we take advantage of the Smolyak sparse grid algorithm to develop a generic robust quantum control scheme in the presence of uncertainties [26]. By taking into account the level of robustness as a weighted tensor product quadrature, higher accuracy and reduced computational cost can be achieved. In the remainder of the paper, we first introduce the mathematical model of quantum control systems with uncertainties, and explain how the Smolyak algorithm assisted gradient-based methods can be formulated. The features and superiority of the proposed scheme are demonstrated in Sections 3 and 4 in the context

of robust control problems. To be specific, by utilizing **smGOAT** or **smGRAPE**, the robustness of state transfer in a two-level quantum system with detuning can be enhanced. For robust realization of a single-qubit gate (the Hadamard gate, the $\pi/8$ gate, the phase gate and the $R_x(\pi)$ gate) or a CNOT gate with uncertainties involved, the level of robustness quantified by infidelity can reach the order of 10^{-4} for a wide range of disturbances. And finally, Section 5 provides the concluding remarks.

2 Robust quantum control based on the Smolyak algorithm

Before we expound the Smolyak algorithm assisted gradient-based methods **smGOAT** and **smGRAPE**, the mathematical framework of quantum control systems in the presence of uncertainties or disturbances will first be provided.

2.1 Quantum control systems with uncertainties

The dynamics of quantum systems with uncertainties involved obey the following Schrodinger equation

$$\frac{dU(t)}{dt} = -iH(t, u, \delta)U(t), \quad (1)$$

where the unitary propagator $U(t)$ starts from the identity operator (i.e. $U(0) = I$), and the Planck constant \hbar is set to be 1. The total Hamiltonian $H(t, u, \delta)$, with the control signals u and uncertainties δ embedded, can be given by

$$H(t, u, \delta) = H_0 + \sum_j u_j(t)H_{cj} + \sum_l \delta_l(t)V_l, \quad (2)$$

where H_0 , H_{cj} , V_l represent the free Hamiltonian, the control Hamiltonian related to the control signal u_j , and the Hamiltonian related to the uncertainty δ_l , respectively. There are different ways to evaluate the control performance, and three commonly used performance indices are listed below,

$$\Phi_1(U_F, U(T)) = \|U_F - U(T)\|^2, \quad (3a)$$

$$\Phi_2(U_F, U(T)) = \min_{\varphi} \|U_F - e^{i\varphi}U(T)\|^2, \quad (3b)$$

$$\Phi_3(U_F, U(T)) = 1 - \left| \frac{1}{\dim} \text{Tr}(U_F^\dagger U(T)) \right|^2. \quad (3c)$$

Here, $\|U\|^2 := \text{Tr}(U^\dagger U)$ for any unitary operator U , U_F denotes the desired propagator, and $U(T)$ denotes the propagator of the system at the end time T . In Eq. (3b), an arbitrary global phase φ is allowed at the end time T . In Eq. (3c), \dim denotes the dimension of the system. In particular, if the uncertainties characterized by δ can be parameterized as a function f of independent random variables collected in $\varepsilon = (\varepsilon_1, \dots, \varepsilon_d)$ with the distribution $P(\varepsilon)$, then by taking the expectation over the

spaces of random variables Ω , the robust control performance index can be rewritten as

$$I_d(\Phi) = \mathbb{E}[\Phi(U_F, U_\varepsilon)] = \int_{\Omega} P(\varepsilon)\Phi(U_F, U_\varepsilon)d\varepsilon, \quad (4)$$

where the propagator $U_\varepsilon(t)$, containing random variables, follows $i\frac{dU_\varepsilon(t)}{dt} = H(t, u, f(\varepsilon))U_\varepsilon(t)$ ($f(\varepsilon)$ denotes the parameterization function). In most cases, it is too time-consuming or complicated to precisely obtain an explicit analytic form of $I_d(\Phi)$, and thus it is reasonable to consider a subset of Ω^d as an approximation. This type of approach can be referred to as a sampling-based algorithm.

Mathematically, the performance index $I_d(\Phi)$ can be viewed as a multidimensional integration with the weighting function $P(\varepsilon)$, thus it can be approximated by a multivariate quadrature of the weighted tensor product,

$$\begin{aligned} I_d(\Phi) &\approx \bar{Q}_1^{n_1} \otimes \cdots \otimes Q_d^{n_d} \Phi \\ &= \sum_{j_1=1}^{n_1} \cdots \sum_{j_d=1}^{n_d} w_{1,j_1} \cdots w_{d,j_d} \Phi(\varepsilon_{1,j_1}, \cdots, \varepsilon_{d,j_d}), \end{aligned} \quad (5)$$

where \otimes denotes the tensor product, and the k -th one-dimensional quadrature $Q_k^{n_k}$ with the order n_k provides a set of nodes $\{\varepsilon_{k,j_k}\}$ and the corresponding weights w_{k,j_k} ($1 \leq j_k \leq n_k$). A different choice of the quadrature rule gives rise to a different sampling set $\mathcal{S} = \{(\varepsilon_{1,j_1}, \cdots, \varepsilon_{d,j_d}) | 1 \leq j_k \leq n_k, 1 \leq k \leq d\}$. If the trapezoidal quadrature rule is adopted with the boundary points removed, the set \mathcal{S} of the above tensor product can be made exactly the sampling set as discussed in [20, 22].

2.2 Smolyak algorithm assisted robust control

Smolyak algorithm provides an efficient approach to reducing the number of nodes in the tensor product. We will show how it can be applied to robust quantum control in this section. To be specific, for a linear operator L with a convergent approximation sequence $L^j (j = 0, 1, \cdots)$, the tensor product of such operators can be written in terms of difference operators, namely

$$L_1 \otimes \cdots \otimes L_d = \sum_{j_1=0}^{\infty} \Delta_1^{j_1} \otimes \cdots \otimes \sum_{j_d=0}^{\infty} \Delta_d^{j_d}, \quad \begin{cases} \Delta_k^{j_k} = L_k^{j_k} - L_k^{j_k-1} & (j_k \geq 1) \\ \Delta_k^0 = L_k^0 = 0 & (j_k = 0) \end{cases}. \quad (6)$$

The core idea of Smolyak algorithm can be interpreted as finding a proper subset \mathcal{I} of multi-index (j_1, \cdots, j_d) , called the Smolyak sparse grid, to approximate the tensor product as precisely as possible and reduce the computational cost at the same time. Particularly, The Smolyak-type quadrature of the following form,

$$A(q, d) = \sum_{(j_1, \cdots, j_d) \in \mathcal{I}(q, d)} \Delta_1^{j_1} \otimes \cdots \otimes \Delta_d^{j_d}, \quad (7)$$

can provide a subset \mathcal{I} and the corresponding upper error bound when the order of the sequence L^j is at most q , with $\mathcal{I}(q, d) = \{(j_1, \cdots, j_d) : j_1 + \cdots + j_d \leq q\}$. It is

more convenient in programming to reformulate Eq. (7) as [27]:

$$A(K, d) = \sum_{\max(K, d) \leq S_j \leq K+d-1} (-1)^{K+d-1-S_j} \binom{d-1}{S_j-K} L_1^{j_1} \otimes \dots \otimes L_d^{j_d}. \quad (8)$$

Here, $S_j = j_1 + \dots + j_d$ ($j_k \geq 1$), and $\binom{d-1}{S_j-K}$ is a binomial number. The parameter $K = q - (d - 1)$ defines the sparse grid level. Especially, when L is taken as the Gaussian quadrature, the quadrature $A(K, d)(\Phi)$ is precise for all polynomials defined on the spaces $P_{k_1} \otimes \dots \otimes P_{k_d}$ with $k_1 + \dots + k_d = 2K - 1$. Details about the error bound and the cost of the Smolyak algorithm can be found in [27, 28].

The control performance index $I_d(\Phi)$ defined in Eq. (4) can then be approximated by

$$I_d(\Phi) \approx A(K, d)(\Phi) = \sum_{\boldsymbol{\varepsilon} = (\varepsilon_{1,j_1}, \dots, \varepsilon_{d,j_d}) \in \mathcal{S}(K, d)} w_{\boldsymbol{\varepsilon}} \Phi(U_F, U_{\boldsymbol{\varepsilon}}), \quad (9)$$

where the abscissas (nodes) $\boldsymbol{\varepsilon} = (\varepsilon_{1,j_1}, \dots, \varepsilon_{d,j_d})$ are taken from the Smolyak sparse grid $\mathcal{S}(K, d) = \{(\varepsilon_{1,j_1}, \dots, \varepsilon_{d,j_d}) : (j_1, \dots, j_d) \in \mathcal{I}(q, d)\}$, with $w_{\boldsymbol{\varepsilon}}$ the corresponding weight. As shown in Fig. 1, for Gauss-Legendre quadrature over the interval $[-0.5, 0.5]$ with the weighting function $P(\boldsymbol{\varepsilon}) \equiv 1$, the associated abscissas and the weights of the Smolyak algorithm are distributed sparsely in space. Furthermore, the precision of the tensor product can increase as the sparse level K increases. Compared to the typical tensor product quadrature with $O(n^d)$ points when there are n nodes in each dimension, the Smolyak sparse grid method employs a much smaller number of points, namely $O(n(\log n)^{d-1})$ points. Therefore, an efficient and relatively accurate estimate can be guaranteed by taking the sample set as the Smolyak sparse grid $\mathcal{S}(K, d)$. Please note that for any n -th order moment of the measure that quantifies the control performance, that is, $\mathbb{E}[\Phi^n(U_F, U_{\boldsymbol{\varepsilon}})]$, an estimate can be obtained using the Smolyak algorithm $A(K, d)(\Phi^n)$ with a sparse level K , through optimization via multi-objective algorithms.

The performance index $\mathbb{E}[\Phi] = I_d(\Phi)$ used in this paper to quantify the robustness in quantum control can be optimized numerically. The related optimization algorithms can, in general, be divided into two classes. One is the class of gradient-based methods, such as widely used **GRAPE** [29] and **GOAT** [30]. The other is the class of gradient-free methods that include, but are not limited to **CRAB** [31]. A sharing step of the above-mentioned algorithms involves calculating the measure of a specific type that quantifies the control performance. Our idea can be briefly interpreted as substituting the original measure with the approximate one in the presence of uncertainties or disturbances. For example, by employing the Smolyak approximation, the cost function in **CRAB** can be written as

$$\mathcal{F} = \alpha A(K, d)(\Phi) + \sum_j \beta_j \mathcal{C}_j[u_j(t)], \quad (10)$$

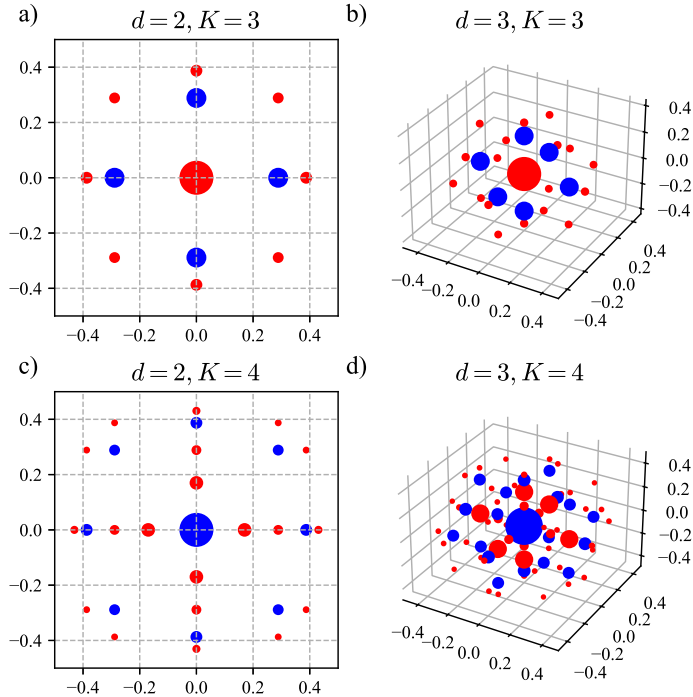


Fig. 1 Demonstration of abscissas (nodes) and weights of Smolyak sparse grids with respect to Gauss-Legendre quadrature rule, when (a) $d=2$ and $K=3$, (b) $d=3$ and $K=3$, (c) $d=2$ and $K=4$, (d) $d=3$ and $K=4$, respectively (the number of random variables that take values according to the axes is d). The color and size of circles correspond to the signs of weights and their absolute values (the color blue and red correspond to the minus and positive signs respectively).

where α and β_j are the associated coefficients, with \mathcal{C}_j denoting the constraints on the control signals. In the implementation of **GRAPE**, we have that

$$u(t) \mapsto u(t) + \eta \frac{\partial A(K, d)(\Phi)}{\partial u(t)}, \quad (11)$$

where η is the learning rate. Additionally, when applying Smolyak algorithm on **GOAT**, the original derivative $\frac{\partial \Phi}{\partial a}$ with respect to the parameter a should be replaced with $\frac{\partial A(K, d)(\Phi)}{\partial a}$.

Without loss of generality, we consider the control signals in the form of Fourier series that can be conveniently implemented in practice as follows,

$$u_j(t) = G(t) \left(a_{0,j} + \sum_{n_u=1}^N a_{n_u,j} \cos\left(\frac{2n\pi t}{T_p}\right) + \sum_{n_u=1}^N b_{n_u,j} \sin\left(\frac{2n\pi t}{T_p}\right) \right). \quad (12)$$

Here, the cycle time T_p , together with the envelope function $G(t)$, can enforce the boundary conditions, that is, $u_j(t) \rightarrow 0$, $\frac{du_j}{dt} \rightarrow 0$ when $t \rightarrow 0$ and $t \rightarrow T_p$. In particular,

$G(t) = \sin^2\left(\frac{\pi t}{T_p}\right)$ can be used as the pulse envelope to satisfy the above conditions. In the following sections, the gradient-based **GOAT** and **GRAPE** with the Smolyak algorithm will be used to optimize the control performance, referred to as **smGOAT** and **smGRAPE** for short, respectively. Furthermore, gradient-based methods can be accelerated by Adam [32] for **GRAPE** and L-BFGS-B [33] for **GOAT**, thus they will be integrated into the implementation. We also normalize the weights appearing in Smolyak sparse grids to make sure their sum is equal to 1.

3 Robust state transfer in a qubit

In this section, in order to illustrate the performance of **smGOAT** proposed in our paper, we consider state transfer in a two-level system (qubit) with static detuning, which has been considered in many existing works [10, 13, 34]. The system Hamiltonian in the resonant regime based on the rotating wave approximation can be given by

$$H(t) = \frac{\Delta}{2}\sigma_z + \frac{1}{2}u_x(t)\sigma_x, \quad (13)$$

where σ_x and σ_z are Pauli operators, and u_x denotes the control signal. The parameter Δ represents the static detuning between the qubit and the driving field. The aim of control is to flip the initial state $|0\rangle$ to $|1\rangle$ allowing for a global phase at the end time T . We thus intend to achieve the population transfer $P = |\langle 1|\phi_T\rangle|^2$ as large as possible, with $|\phi_T\rangle$ being the final quantum state. Assume that the detuning Δ remains small subject to a specific distribution during evolution, and then we can proceed with a sparse tensor product. Note that when $K = 1$, the sparse grid is reduced to a one-dimensional quadrature. In terms of the configuration of the parameters in our simulation, the time duration of evolution T is set to 8, with $T_p = 8$ as well. The number of Fourier bases for the control signal is chosen as $N = 5$. In particular, the parameters $\{a_i\}$ and $\{b_i\}$ of the control signal u_x will be uniformly randomized in the interval $[-0.5, 0.5]$ as the initial guess for **smGOAT**.

We consider two possible circumstances of detuning Δ in this robust control problem. One is based on a uniform distribution as $\Delta \sim \mathbb{U}(-0.5, 0.5)$, and the other follows a normal distribution as $\Delta \sim \mathbb{N}(0, \zeta^2)$ with $\zeta = 0.4$. Consequently, we take the quadrature rule L as Gauss-Legendre and Gauss-Hermite, respectively. The robustness of the system can be visualized with respect to different values of the detuning Δ in Fig. 2. Obviously, it can be seen that remarkable robustness quantified by $1 - P$ can be achieved at the level of 10^{-4} within a wide range of detuning. Smooth control signals can make population transfer values P flat in the range $[-1.0, 1.0]$ for the detuning Δ according to both quadrature rules. In contrast, the standard Rabi frequency is quite sensitive to uncertainties. Note that the Gauss-Legendre rule concentrates its samples within the interval $[-0.5, 0.5]$ as scheduled and can reach $\mathbb{E}[1 - P] \approx 5.66 \times 10^{-8}$ for $K = 4$ and $\mathbb{E}[1 - P] \approx 7.26 \times 10^{-8}$ for $K = 6$, while the Gauss-Hermite rule scatters its samples widely and can reach $\mathbb{E}[1 - P] \approx 5.17 \times 10^{-5}$ for $K = 4$ and $\mathbb{E}[1 - P] \approx 2.02 \times 10^{-6}$ for $K = 6$. In principle, one may estimate the expectation and its gradient more precisely as the sparse level (the number of nodes) increases, but it is not always true for the enhancement of performance. Please also note that some

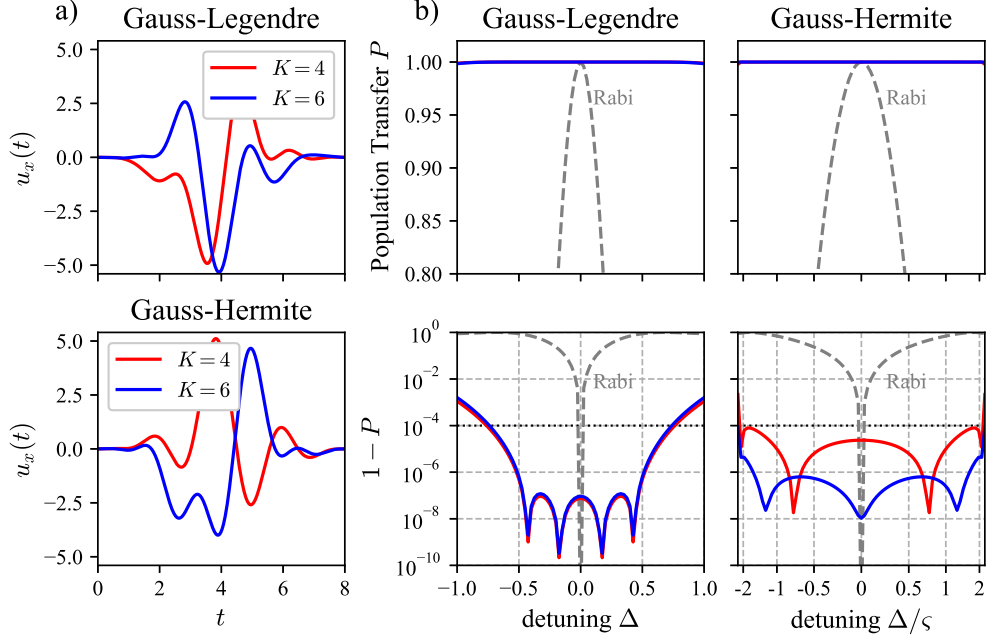


Fig. 2 Results of the Gauss-Legendre and Gauss-Hermite quadrature rules with different sparse level K (i.e. red lines for $K = 4$ and blue lines for $K = 6$), with the control signals plotted in (a) and the population transfer P as well as $1 - P$ using a logarithmic scale plotted in (b). The robustness profile of Rabi frequency is also plotted in (b) (black dashed lines) for comparison. For the Gauss-Hermite quadrature, the x-axis is scaled according to probability density function with $\varsigma = 0.4$.

sharp declines in Fig. 2 (b) have a weak correlation with the distribution of sampling points, which is consistent with the characteristics of sampling-based methods. The related parameters of the control signals are detailed in Table 1.

4 Robust realization of a quantum gate

In this section we will show how ultrahigh fidelity quantum gates can be realized using the Smolyak algorithm assisted robust quantum control method.

4.1 Robust realization of a single-qubit gate

Firstly, a single-qubit high-fidelity gate will be realized in the presence of uncertainty. We take into account three gates of significant interest in quantum computing, namely the Hadamard gate U_H and the $\pi/8$ gate $U_{\pi/8}$ and the phase gate U_S [35]:

$$U_H = \frac{1}{\sqrt{2}} \begin{bmatrix} 1 & 1 \\ 1 & -1 \end{bmatrix}, U_{\pi/8} = \begin{bmatrix} 1 & 0 \\ 0 & e^{i\pi/4} \end{bmatrix}, U_S = \begin{bmatrix} 1 & 0 \\ 0 & i \end{bmatrix}. \quad (14)$$

The system propagator is supposed to evolve initially from $U(0) = I$ to the target gate U_F , allowing for an arbitrary phase factor. Therefore, the robustness can be evaluated

Table 1 Fourier coefficients of the control signals (The first and second lines under the item 'Parameters' correspond to the values of $\{a_j\}$ and $\{b_j\}$ as prescribed in Eq. (12).)

Target	Quadrature	K	Pulse	Parameters	
1⟩	Gauss-Legendre	4	u_x	[-0.541266, 0.4879911, 0.1914271, 0.64949, -0.1146768, 0.3331206]	
		6		[-1.6554518, 1.1507073, -0.958743, 1.1844206, -0.640326]	
	Gauss-Hermite	4		[0.6924232, -0.7128341, -0.6771369, 0.376103, -0.3724295]	
		6		[0.345237, -0.8754605, 0.563588, -1.0765119, 1.704442, -0.0775378]	
				4	[0.7466213, -0.0696301, 1.2401343, -0.4713429, 0.0319697]
				6	[-0.6848944, 0.2011103, -0.289895, 0.5335654, -0.7945864, 1.308883]
				[-1.516149, 2.3847856, -0.377001, -0.0110573, 0.5945622]	
U_H	Gauss-Legendre	4	u_x	[-1.10205484, -0.16444018, 0.356119, 1.80099137]	
			u_y	[0.74186792, -1.1333456, -1.22726687]	
$U_{\pi/8}$	Gauss-Legendre	4	u_x	[2.24002595, 3.0787707, -0.54292804, -1.32754733]	
			u_y	[2.01127864, 1.7822432, 1.51006954]	
U_S	Gauss-Legendre	4	u_x	[-1.97064098, -4.01920656, 0.31203617, 0.8928809]	
			u_y	[1.06616553, 1.28528487, 0.20736214]	
$R_x(\pi)$	Gauss-Legendre	3	u_x	[2.39685112, 4.87430845, -0.56553063, -1.26091625]	
			u_y	[0.97969155, 1.14522837, 0.38519095]	
$R_x(\pi)$	Gauss-Legendre	4	u_x	[-1.59137647, -3.52012761, 1.21916556, 1.10448505]	
			u_y	[-1.87008537, -2.18823133, -0.63684599]	
			3	u_x	[-1.28230799, -2.89252763, 0.8221858, 0.63479593]
				u_y	[2.00875836, 2.18907434, 0.05213139]
			4	u_x	[0.5286695, 0.88444058, 1.27386703, 0.60613856]
				u_y	[0.70152979, 1.12258258, 0.77939379]
		4	u_x	[-0.9268824, -0.87491169, 0.15829603, 0.11848552]	
			u_y	[-0.45997346, -0.70470614, -0.35510744]	
				[-0.46720312, -0.51100983, -1.41384471, -0.55770797]	
				[0.39306135, 0.7920471, 0.56493162]	
				[-1.329766, -1.79146926, -0.52194291, -0.37675494]	
				[0.50968566, 0.77403372, 0.65863078]	

by the measure defined in Eq. (3b). The system Hamiltonian of the following form is steered by two control signals $u_x(t)$ and $u_y(t)$, with uncertainty involved [36]:

$$H(t) = \frac{\Delta}{2}\sigma_z + (1 + \delta) \left(\frac{1}{2}u_x(t)\sigma_x + \frac{1}{2}u_y(t)\sigma_y \right), \quad (15)$$

where Δ is the detuning and δ characterizes the uncertainty (along the control amplitude $\sqrt{u_x^2 + u_y^2}$). Assuming that the detuning Δ and the uncertainty δ follow the same uniform distribution, i.e. $\Delta, \delta \sim \mathbb{U}(-0.1, 0.1)$, we proceed with the Gauss-Legendre quadrature rule to perform the approximation.

In the numerical simulation, we set the time parameters $T = T_p = 10$, the number of Fourier bases $N = 3$, and the sparse level $K = 4$ that is adequate for the number of random variables $d = 2$. Considering the control signals expanded by the Fourier series as provided in Eq. (12), the robust control performance, with respect to the Hadamard gate, the $\pi/8$ gate, and the phase gate, can be observed in Fig. 3. It is worth mentioning that the control pulses obtained whose trajectories are smooth during the whole dynamic process can be easily implemented in experiments. Bearing

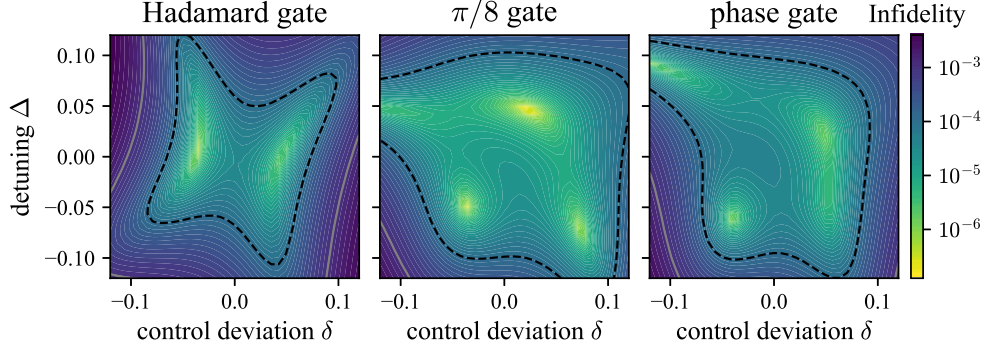


Fig. 3 Landscapes quantifying the robustness, corresponding to the Hadamard gate U_H , the $\pi/8$ gate $U_{\pi/8}$, and the phase gate U_S , respectively. The grey solid and black dashed lines in the landscapes represent the levels of robustness quantified by infidelity at 10^{-3} and 10^{-4} respectively.

in mind that the infidelity of effective quantum gates should be of the order 10^{-4} , the uncertainty existing in the system, such as detuning or deviation of control parameters, is detrimental to the control performance. Fortunately, with the help of **smGOAT**, the region enclosed by the robustness level 10^{-4} (the region enclosed by the black dashed line in Fig. 3) is evidently expanded, and the resulting averaged infidelity $\mathbb{E}[\Phi]$ for the three gates is around 1.87×10^{-4} , 4.18×10^{-5} , 7.35×10^{-5} , respectively. This indeed verifies that **smGOAT** has a better tolerability of uncertainty.

In the following, we are concerned with the scenario in which disturbances are allowed in all directions (x , y , and z). The system Hamiltonian can thus be written as

$$H(t) = \frac{1}{2}u_x(t)\sigma_x + \frac{1}{2}u_y(t)\sigma_y + \frac{1}{2}\delta_x\sigma_x + \frac{1}{2}\delta_y\sigma_y + \frac{1}{2}\delta_z\sigma_z, \quad (16)$$

where $\delta_{\{x,y,z\}}$ are independent disturbances during the evolution, and the dynamics can be manipulated through x and y . In this case, the target gate $R_x(\pi) = -i\sigma_x$ that can rotate the qubit along the x direction with an angle of π is supposed to be realized within the gate time $T = 50$. The discrepancy between the target gate U_F and the final gate U_T as defined in Eq. (3a) is used to quantify the level of robustness. The remaining settings of **smGOAT** are analogous to the previous example. In addition, the number of Fourier bases is $N = 3$, and the sparse level is $K = 3$ or $K = 4$.

The simulation results on robust realization of the $R_x(\pi)$ gate using **smGOAT** have been demonstrated in Fig. 4, compared to the geometric method (denoted by **Ref.** in Fig. 4.) discussed in [7, 8]. To be specific, 800 tests of all directional disturbances uniformly sampled from cubic space $[-0.05, 0.05]^3$ are represented by the black dots in Fig. 4 (b). It can be seen that the worst performance given by **smGOAT** is much better than that given by the geometric method. More specifically, the worst infidelity can be reduced 8 times for $K = 3$ and 20 times for $K = 4$ by **smGOAT**. In addition, the averaged infidelity $\mathbb{E}[\Phi]$ provided by **smGOAT** is around 2.05×10^{-3} for $K = 3$ and 6.5×10^{-4} for $K = 4$. The control pulses in the presence of all directional disturbances are also plotted in Fig. 4 (a). Furthermore, Fig. 4 (c) shows the landscapes comparing the robust control performances between the geometric method and **smGOAT** with

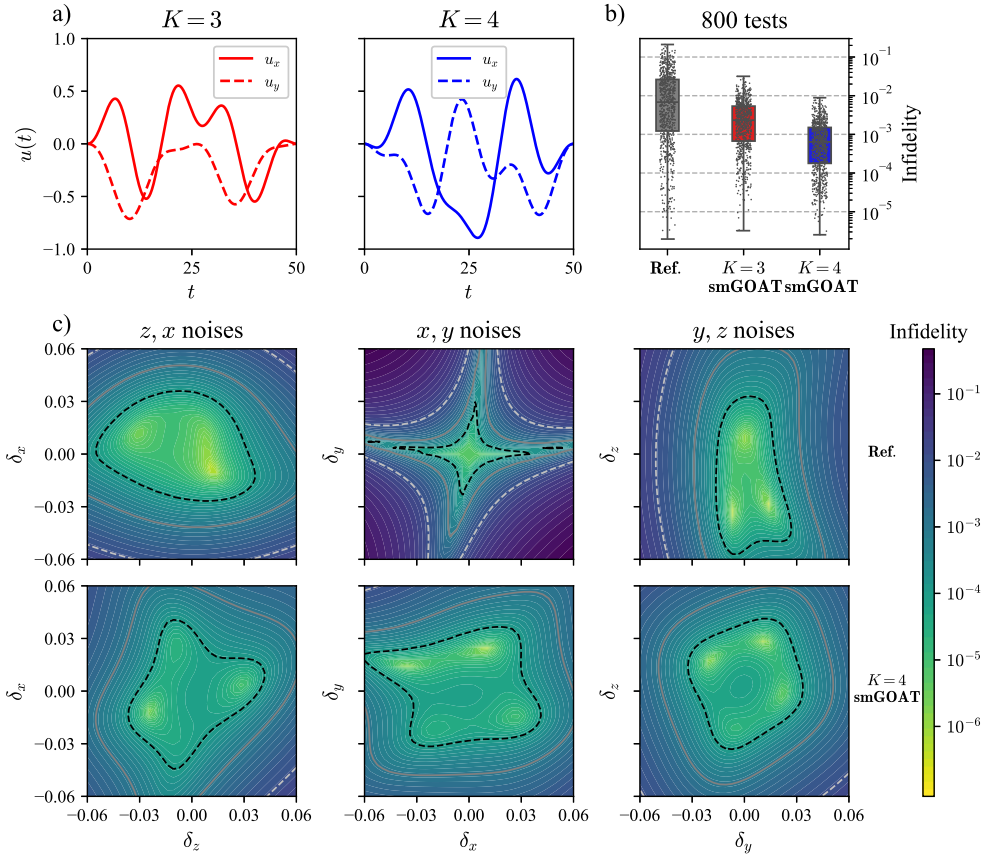


Fig. 4 Simulation results regarding robust realization of the $R_x(\pi)$ gate are depicted. The level of robustness quantified by infidelity when noises or disturbances exist in two directions ($z-x$, $x-y$ and $y-z$) is plotted in (c) (the white dashed, grey solid and black dashed lines correspond to the infidelity values at 10^{-2} , 10^{-3} and 10^{-4} , respectively), and values of infidelity through 800 tests of all directional disturbances uniformly sampled from cubic space $[-0.05, 0.05]^3$ are box-plotted in (b) (the grey, red and blue boxes correspond to the cases **Ref.**, **smGOAT** with $K=3$, and **smGOAT** with $K=4$, respectively). The control trajectories in the presence of all directional disturbances are also plotted in (a) (the red and blue lines correspond to the cases $K=3$ and $K=4$ respectively).

$K=4$ in the presence of two directional noises or disturbances. Both **Ref.** and **smGOAT** present similarly satisfying robustness with disturbances involved in the y and z directions or in the z and x directions. However, when there are disturbances in the x and y directions, **smGOAT** outperforms **Ref.** since the region enclosed by the robustness level 10^{-4} (the region enclosed by the black dashed line in Fig. 4 (c)) obtained by **smGOAT** is obviously larger than that obtained by **Ref.**. The form of the objective function associated with the geometric method intrinsically constrains the robustness in such a scenario, which thus leads to a squeezed and shrunken region enclosed by the robustness level 10^{-4} or 10^{-3} . This example particularly shows the advance of the sampling-based method **smGOAT** in obtaining stronger robustness when multiple disturbances are involved.

4.2 Robust realization of a CNOT gate

In this section, we focus on the robust realization of the CNOT gate (i.e. $U_{\text{CNOT}} = |00\rangle\langle 00| + |01\rangle\langle 01| + |11\rangle\langle 10| + |10\rangle\langle 11|$), without correcting errors using local z phases. The system Hamiltonian can then be given by

$$H(t, u, \delta) = \sigma_{z,1}\sigma_{z,2} + \delta_1\sigma_{z,1} + \delta_2\sigma_{z,2} + \sum_{j=1}^2 [u_{x,j}(t)\sigma_{x,j} + u_{y,j}(t)\sigma_{y,j}], \quad (17)$$

where $\sigma_{\{x,y,z\},j}$ are the Pauli operators corresponding to the j -th qubit, in the presence of system uncertainties described by δ_1 and δ_2 appearing on each qubit. Here, the uncertainties are assumed to follow the normal distribution, namely $\delta_1, \delta_2 \sim \mathcal{N}(0, \varsigma^2)$. The performance index defined in Eq. (3c) will be used to quantify the level of fidelity. In order to demonstrate applicability of Smolyak sparse grids for different optimization algorithms, apart from **smGOAT**, **smGRAPE**) will be applied to robustly control a CNOT gate. Because the piecewise control protocol requires segmentation of the time duration, we set the time length $T = 10$ and the associated number of steps $N = 100$.

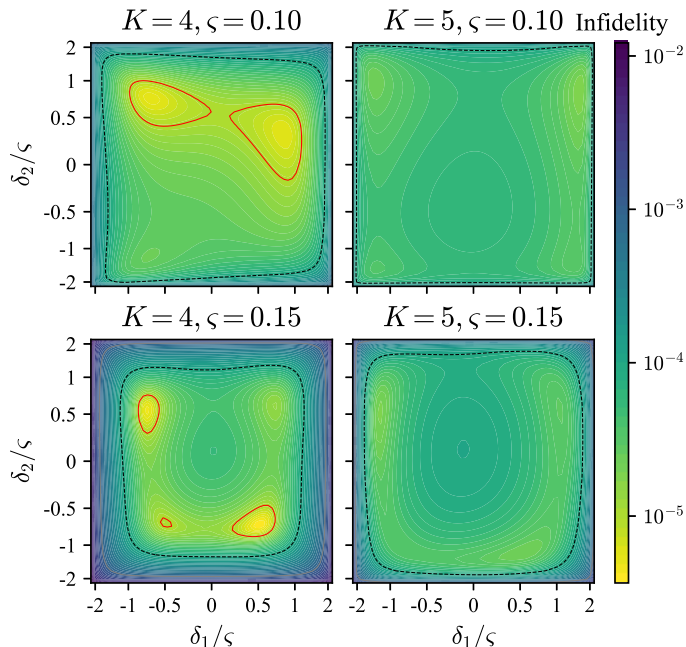


Fig. 5 Landscapes demonstrating the control performance of the CNOT gate using **smGRAPE** against static detunings δ_1 and δ_2 , with the sparse level $K = 4, 5$ and deviations $\varsigma = 0.10, 0.15$ (error correction with local z phases is not involved). The grey solid lines, the black dashed lines and the red solid lines correspond to the infidelity values at 10^{-3} , 10^{-4} and 10^{-5} , respectively. The axes, corresponding to the values of ς , are scaled according to the probability density of uncertainty in order to better interpret the robustness.

Since the Smolyak algorithm is essentially sample-based, choices of the sparse level K and the parameterization $f(\varepsilon)$ (as prescribed in Eq. (4)) of $\delta_{1(2)}$ can influence the number and spatial position of samples. Experimentally for multiple uncertainties, it is not always true that the control performance of the Smolyak-assisted algorithm can be improved as the sparse level K increases. For that reason, we compare the control performance of **smGRAPE** in different scenarios with $K = 4, 5$ and $\varsigma = 0.10, 0.15$, as demonstrated in Fig. 5. A higher value of the deviation ς ($\varsigma = 0.15$) which gives $\delta_{1(2)} = \varsigma\varepsilon$ ($\varepsilon \sim \mathbb{N}(0, 1)$) implies a wider range of samples, such that the region of infidelity bounded by 10^{-4} is larger (note that the true value along the axis is divided by ς). When we keep the deviation value ς , a higher value of the sparse level K ($K = 5$) also implies that more samples should be considered. Consequently, the averaged fidelity within a broader range can be improved, but maximal fidelity might suffer a decrease. Although **smGRAPE** can attain ultralow infidelity down to the order of 10^{-4} together with strong robustness, the applicability of **smGRAPE** might be limited in the situation where only the simple form of driving fields is available.

5 Conclusion

In summary, inspired by the Smolyak sparse grid algorithm, we develop a robust control scheme to deal with challenging difficulties in quantum technologies. This scheme can help improve the robustness of various quantum optimal control algorithms, including but not limited to **GRAPE** and **GOAT**. Compared to other robust quantum control schemes, the Smolyak algorithm assisted parametric scheme provides a universal sampling methodology with less computational workload and stronger robustness.

In more concrete terms, the Smolyak sparse grid algorithm has been merged with gradient-based optimization methods such as **GOAT** and **GRAPE**, referred to as **smGOAT** and **smGRAPE** in our work, with successful applications to robust control problems regarding quantum state regulation and realization of quantum gates. For example, by utilizing **smGOAT** or **smGRAPE**, the robustness of state transfer in a two-level quantum system with detuning can be enhanced. In terms of robust realization of a single-qubit gate (the Hadamard gate, the $\pi/8$ gate, the phase gate and the $R_x(\pi)$ gate) or a CNOT gate in the presence of uncertainties or disturbances, the level of robustness quantified by infidelity can easily reach the order of 10^{-4} subject to a wide range of deviations, with smooth control signals provided.

Although the proposed sampling-based robust control scheme presents superiority (e.g. reduced computational cost and wider ultrahigh fidelity region), the number of samples is still large for complicated mixed uncertainties. Our future work may include considering totally time-varying disturbances, proving convergence of our algorithm rigorously, and further improving the efficiency, contributing to the development of more reliable quantum computing and communication.

Acknowledgements

This work was supported by the National Natural Science Foundation of China (Grants Nos. 62003113, 62173296 and 62273016), and Shenzhen Science and Technology Program (Grants No. KQTD20200820113010023).

References

- [1] Koch, C.P., Boscain, U., Calarco, T., Dirr, G., Filipp, S., Glaser, S.J., Kosloff, R., Montangero, S., Schulte-Herbrüggen, T., Sugny, D., Wilhelm, F.K.: Quantum optimal control in quantum technologies. strategic report on current status, visions and goals for research in europe. EPJ Quantum Technology **9**(1), 19 (2022) <https://doi.org/10.1140/epjqt/s40507-022-00138-x> . Accessed 2024-05-18
- [2] Weidner, C.A., Reed, E.A., Monroe, J., Sheller, B., O’Neil, S., Maas, E., Jonckheere, E.A., Langbein, F.C., Schirmer, S.G.: Robust Quantum Control in Closed and Open Systems: Theory and Practice (2024). <https://arxiv.org/abs/2401.00294>
- [3] Zeng, J., Yang, C.H., Dzurak, A.S., Barnes, E.: Geometric formalism for constructing arbitrary single-qubit dynamically corrected gates. Physical Review A **99**, 052321 (2019) <https://doi.org/10.1103/PhysRevA.99.052321>
- [4] Buterakos, D., Das Sarma, S., Barnes, E.: Geometrical formalism for dynamically corrected gates in multiqubit systems. PRX Quantum **2**, 010341 (2021) <https://doi.org/10.1103/PRXQuantum.2.010341>
- [5] Dong, W., Zhuang, F., Economou, S.E., Barnes, E.: Doubly geometric quantum control. PRX Quantum **2**, 030333 (2021) <https://doi.org/10.1103/PRXQuantum.2.030333>
- [6] Barnes, E., Calderon-Vargas, F.A., Dong, W., Li, B., Zeng, J., Zhuang, F.: Dynamically corrected gates from geometric space curves. Quantum Science and Technology **7**(2), 023001 (2022) <https://doi.org/10.1088/2058-9565/ac4421>
- [7] Hai, Y.-J., Li, J., Zeng, J., Deng, X.-H.: Universal robust quantum gates by geometric correspondence of noisy quantum dynamics (2022)
- [8] Yi, K., Hai, Y.-J., Luo, K., Chu, J., Zhang, L., Zhou, Y., Song, Y., Liu, S., Yan, T., Deng, X.-H., Chen, Y., Yu, D.: Robust quantum gates against correlated noise in integrated quantum chips. Phys. Rev. Lett. **132**, 250604 (2024) <https://doi.org/10.1103/PhysRevLett.132.250604>
- [9] Daems, D., Ruschhaupt, A., Sugny, D., Guérin, S.: Robust quantum control by a single-shot shaped pulse. Phys. Rev. Lett. **111**, 050404 (2013) <https://doi.org/10.1103/PhysRevLett.111.050404>

- [10] Dridi, G., Liu, K., Guérin, S.: Optimal robust quantum control by inverse geometric optimization. *Phys. Rev. Lett.* **125**, 250403 (2020) <https://doi.org/10.1103/PhysRevLett.125.250403>
- [11] Laforgue, X., Dridi, G., Guérin, S.: Optimal quantum control robust against pulse inhomogeneities: Analytic solutions. *Phys. Rev. A* **106**, 052608 (2022) <https://doi.org/10.1103/PhysRevA.106.052608>
- [12] Kosut, R.L., Grace, M.D., Brif, C.: Robust control of quantum gates via sequential convex programming. *Phys. Rev. A* **88**, 052326 (2013) <https://doi.org/10.1103/PhysRevA.88.052326>
- [13] Van Damme, L., Ansel, Q., Glaser, S.J., Sugny, D.: Robust optimal control of two-level quantum systems. *Phys. Rev. A* **95**, 063403 (2017) <https://doi.org/10.1103/PhysRevA.95.063403>
- [14] Poggi, P.M., De Chiara, G., Campbell, S., Kiely, A.: Universally robust quantum control. *Phys. Rev. Lett.* **132**, 193801 (2024) <https://doi.org/10.1103/PhysRevLett.132.193801>
- [15] Viola, L., Knill, E., Lloyd, S.: Dynamical decoupling of open quantum systems. *Phys. Rev. Lett.* **82**, 2417–2421 (1999) <https://doi.org/10.1103/PhysRevLett.82.2417>
- [16] Genov, G.T., Schraft, D., Vitanov, N.V., Halfmann, T.: Arbitrarily accurate pulse sequences for robust dynamical decoupling. *Phys. Rev. Lett.* **118**, 133202 (2017) <https://doi.org/10.1103/PhysRevLett.118.133202>
- [17] Genov, G.T., Schraft, D., Halfmann, T., Vitanov, N.V.: Correction of arbitrary field errors in population inversion of quantum systems by universal composite pulses. *Phys. Rev. Lett.* **113**, 043001 (2014) <https://doi.org/10.1103/PhysRevLett.113.043001>
- [18] Wu, H.-N., Zhang, C., Song, J., Xia, Y., Shi, Z.-C.: Composite pulses for optimal robust control in two-level systems. *Phys. Rev. A* **107**, 023103 (2023) <https://doi.org/10.1103/PhysRevA.107.023103>
- [19] Guéry-Odelin, D., Ruschhaupt, A., Kiely, A., Torrontegui, E., Martínez-Garaot, S., Muga, J.G.: Shortcuts to adiabaticity: Concepts, methods, and applications. *Rev. Mod. Phys.* **91**, 045001 (2019) <https://doi.org/10.1103/RevModPhys.91.045001>
- [20] Chen, C., Dong, D., Long, R., Petersen, I.R., Rabitz, H.A.: Sampling-based learning control of inhomogeneous quantum ensembles. *Phys. Rev. A* **89**, 023402 (2014) <https://doi.org/10.1103/PhysRevA.89.023402>
- [21] Anderson, B.E., Sosa-Martinez, H., Riofrío, C.A., Deutsch, I.H.,

- Jessen, P.S.: Accurate and robust unitary transformations of a high-dimensional quantum system. *Phys. Rev. Lett.* **114**, 240401 (2015) <https://doi.org/10.1103/PhysRevLett.114.240401>
- [22] Dong, D., Mabrok, M.A., Petersen, I.R., Qi, B., Chen, C., Rabitz, H.: Sampling-based learning control for quantum systems with uncertainties. *IEEE Transactions on Control Systems Technology* **23**(6), 2155–2166 (2015) <https://doi.org/10.1109/TCST.2015.2404292>
- [23] Ge, X., Wu, R.-B.: Risk-sensitive optimization for robust quantum controls. *Phys. Rev. A* **104**, 012422 (2021) <https://doi.org/10.1103/PhysRevA.104.012422>
- [24] Wu, R.-B., Ding, H., Dong, D., Wang, X.: Learning robust and high-precision quantum controls. *Phys. Rev. A* **99**, 042327 (2019) <https://doi.org/10.1103/PhysRevA.99.042327>
- [25] Ge, X., Ding, H., Rabitz, H., Wu, R.-B.: Robust quantum control in games: An adversarial learning approach. *Phys. Rev. A* **101**, 052317 (2020) <https://doi.org/10.1103/PhysRevA.101.052317>
- [26] Smolyak, S.A.: Quadrature and interpolation formulas for tensor products of certain classes of functions. *Doklady Akademii Nauk SSSR* **148**(5), 1042–1045 (1963). Russian Academy of Sciences
- [27] Wasilkowski, G.W., Woźniakowski, H.: Explicit cost bounds of algorithms for multivariate tensor product problems. *Journal of Complexity* **11**(1), 1–56 (1995) <https://doi.org/10.1006/jcom.1995.1001>
- [28] Wasilkowski, G.W., Woźniakowski, H.: Weighted tensor product algorithms for linear multivariate problems. *Journal of Complexity* **15**(3), 402–447 (1999) <https://doi.org/10.1006/jcom.1999.0512>
- [29] Khaneja, N., Reiss, T., Kehlet, C., Schulte-Herbrüggen, T., Glaser, S.J.: Optimal control of coupled spin dynamics: design of nmr pulse sequences by gradient ascent algorithms. *Journal of Magnetic Resonance* **172**(2), 296–305 (2005) <https://doi.org/10.1016/j.jmr.2004.11.004>
- [30] Machnes, S., Assémat, E., Tannor, D., Wilhelm, F.K.: Tunable, flexible, and efficient optimization of control pulses for practical qubits. *Phys. Rev. Lett.* **120**, 150401 (2018) <https://doi.org/10.1103/PhysRevLett.120.150401>
- [31] Caneva, T., Calarco, T., Montangero, S.: Chopped random-basis quantum optimization. *Phys. Rev. A* **84**, 022326 (2011) <https://doi.org/10.1103/PhysRevA.84.022326>
- [32] Kingma, D.P., Ba, J.: Adam: A method for stochastic optimization. In: *International Conference on Learning Representations (ICLR)* (2014)

- [33] Byrd, R.H., Lu, P., Nocedal, J., Zhu, C.: A limited memory algorithm for bound constrained optimization. *SIAM Journal on Scientific Computing* **16**(5), 1190–1208 (1995) <https://doi.org/10.1137/0916069>
- [34] Huang, C.-H., Goan, H.-S.: Robust quantum gates for stochastic time-varying noise. *Phys. Rev. A* **95**, 062325 (2017) <https://doi.org/10.1103/PhysRevA.95.062325>
- [35] Nielsen, M.A., Chuang, I.L.: *Quantum Computation and Quantum Information: 10th Anniversary Edition*. Cambridge University Press, Cambridge (2010). <https://doi.org/10.1017/CBO9780511976667>
- [36] Blais, A., Grimsmo, A.L., Girvin, S.M., Wallraff, A.: Circuit quantum electrodynamics. *Rev. Mod. Phys.* **93**, 025005 (2021) <https://doi.org/10.1103/RevModPhys.93.025005>